Available online at www.sciencedirect.com
ScienceDirect
Journal of Molecular Graphics and Modelling 25 (2006) 324–332
Journal of Molecular Graphics and Modelling
www.elsevier.com/locate/JMGM

Structural and dynamical properties of different protonated states of mutant HIV-1 protease complexed with the saquinavir inhibitor studied by molecular dynamics simulations

Ornjira Aruksakunwong [a], Kitiyaporn Wittayanarakul [a], Pornthep Sompornpisut [a], Vannajan Sanghiran [b], Vudthichai Parasuk [a], Supot Hannongbua [a,*]

[a] *Department of Chemistry, Faculty of Science, Chulalongkorn University, Prathumwan, Bangkok 10330, Thailand*
[b] *Department of Chemistry, Faculty of Science, Chiang Mai University, Chiang Mai 50200, Thailand*

Received 13 July 2005; received in revised form 17 January 2006; accepted 18 January 2006
Available online 28 February 2006

Abstract

To understand the basis of drug resistance, particularly of the HIV-1 PR, three molecular dynamics (MD) simulations of HIV-1 PR mutant species, G48V, complexed with saquinavir (SQV) in explicit aqueous solution with three protonation states, diprotonation on Asp25 and Asp25′ (Di-pro) and monoprotonation on each Asp residue (Mono-25 and Mono-25′). For all three states, H-bonds between saquinavir and HIV-1 PR were formed only in the two regions, flap and active site. It was found that conformation of P2 subsite of SQV in the Mono-25 state differs substantially from the other two states. The rotation about 177° from the optimal structure of the wild type was observed, the hydrogen bond between P2 and the flap residue (Val48) was broken and indirect hydrogen bonds with the three residues (Asp29, Gly27, and Asp30) were found instead. In terms of complexation energies, interaction energy of −37.3 kcal/mol for the Mono-25 state is significantly lower than those of −30.7 and −10.7 kcal/mol for the Mono-25′ and Di-pro states, respectively. It was found also that protonation at the Asp25 leads to a better arrangement in the catalytic dyad, i.e., the Asp25–Asp25′ interaction energy of −8.8 kcal/mol of the Mono-25 is significantly lower than that of −2.6 kcal/mol for the Mono-25′ state. The above data suggest us to conclude that interaction in the catalytic area should be used as criteria to enhance capability in drug designing and drug screening instead of using the total inhibitor/enzyme interaction.

Keywords: HIV-1 protease; Molecular dynamics simulations; Mutation; Protonation state; Saquinavir

1. Introduction

The human immunodeficiency virus type 1 (HIV-1) is the causative agent in acquired immunodeficiency syndrome (AIDS). This disease was recognized in the U.S., around 1981 [1]. There are three essential enzymes involved in the replication cycle of this virus which are reverse transcriptase (RT), protease (PR) and integrase (IN). They are therefore important targets for drug development. Although effective drugs have been developed against HIV-1 PR and HIV-1 RT, however, it was reported that inhibitors at the first target are more potent [2]. Therefore, HIV-1 PR is an attractive target for antiviral therapy. The HIV-1 PR consists of two identical polypeptides of 99 amino acids (Fig. 1), each chain contains an N-terminal Pro and C-terminal Phe. The active site of PR is formed at the dimer interface containing two conserved catalytic dyad, Asp25 and Asp25′ [3]. The substrate binding cleft is composed of equivalent residues from each subunit and is bound on one side by the active site aspartic acids and on the other by the flap region. To date, there are several FDA-approved PR inhibitors in clinical uses and saquinavir is considered to be a highly potent and selective transition state analog inhibitor of the HIV-1 PR [4].

A major problem for the clinical uses of PR inhibitors is the development of drug resistance due to substitutions observed in almost 50% of the residues and over 20 residues associated with resistance to clinically available inhibitors [5]. Recently, the correlation between the inhibitor structure of the HIV-1 PR target and the drug resistance was studied [6]. The kinetic experimental data show that decreased affinity of the

* Corresponding author. Tel.: +66 2 2187603; fax: +66 2 2187603.
E-mail address: supot.h@chula.ac.th (S. Hannongbua).

1093-3263/$ – see front matter © 2006 Elsevier Inc. All rights reserved.
doi:10.1016/j.jmgm.2006.01.004

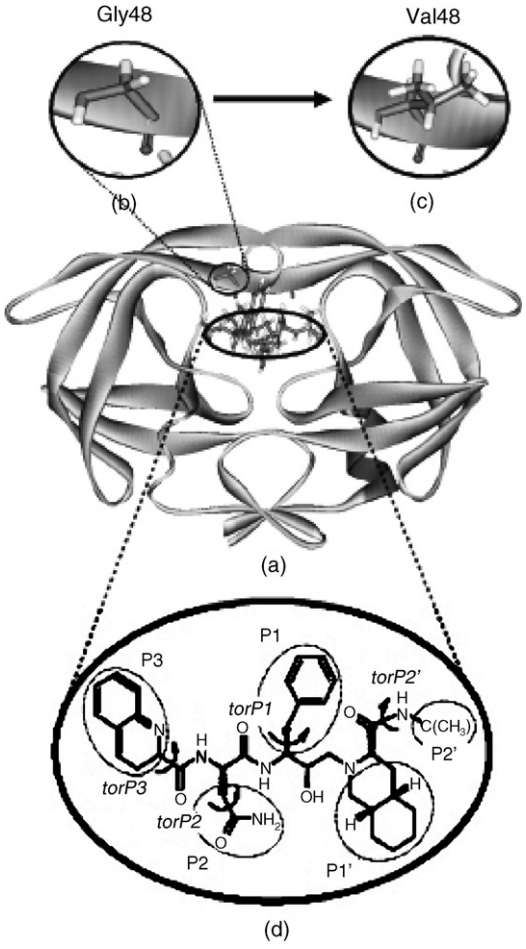

Fig. 1. Schematic representation of the HIV-1 PR complexed with saquinavir (a) in which molecular structure of Gly48 (b) and Val48 (c) in the G48V and of saquinavir (d) were also displayed. Here, P1, P2, P3, P1′ and P2′ subsites are labeled by circle and torsional angle of each subsite was defined by *tor*.

drugs for many mutants is caused primarily by an increase in dissociation rates. The HIV-1 PR mutant species, G48V, is associated in vivo with saquinavir resistance [7]. Residue Gly48 locates in the flap region of the HIV-1 PR and is responsible for the formation of the S2/S2′ and S3/S3′ binding site—the regions of the enzyme that bind with P2/P2′ and P3/P3′ of the inhibitor, respectively [8]. In addition, it was found that Gly48 plays a role in shaping the binding pocket of the active site and stabilizing the enzyme–substrate complex [6]. Substitution of this residue by valine introduces a bulky side chain into the S3/S3′ binding pocket and results in resistance towards saquinavir leading to an increase of the inhibition constant (K_i) value by 13.5-fold [9]. However, this effect was not observed for other inhibitors.

As an aspartic protease, the protonation state of the catalytic aspartic acids, Asp25 and Asp25′, is the key to explain the catalytic mechanism of both wild type and mutant type. Plane wave-based ab initio molecular dynamics calculations [10] as well as NMR measurements [11] of the HIV-1 PR complexed with pepstatin lead to the conclusion that the system is, at least, monoprotonated. In addition, the ab initio calculation method was preformed on the active site of HIV-1 PR and the free energy perturbation (FEP) method was used to determine the binding free energy of four different protonated states of HIV-1 PR complexed with A74704 by Ky-Youb Nam et al. [12]. The results have the potentially significant implications that the complex is monoprotonated on Asp25.

In this study, molecular dynamics simulations of the G48V HIV-1 PR complexed with saquinavir in explicit aqueous solution were carried out. Due to an unclear detailed mechanism of the reaction catalyzed by HIV-1 PR [13], therefore, the simulations have to be performed for all three possible protonation states of the two aspartic residues, Asp25 and Asp25′.

2. Computational method

2.1. Preparation of the initial structures

In order to investigate the relative dynamics properties among different protonation states of the mutant HIV-1 PR complexed with the inhibitor (saquinavir), three MD simulations were preformed, monoprotonate on Asp25 (Mono-25), monoprotonate on Asp25′ (Mono-25′) and diprotonate on both aspartic acids (Di-pro). The crystal structure of saquinavir bound to wild-type protease was taken from the Protein Data Bank PDB (1HXB) [14] and used as the reference structure. Among the two available crystal structures, the first one which are commonly used in literatures [15] was applied for our simulation. All missing atoms of the protein were added using the LEaP module in the AMBER 7 software package [16]. The protonation state of the ionizable residues, the C- and the N-termini, except for D25/25′, was assigned based on the predicted pK_a values at pH 7. The pK_as of ionizable residues were calculated based on the Poisson–Boltzmann free energy calculations. Details of these calculations are given elsewhere [17]. Hydrogen atoms were then added to the two catalytic aspartic residues in order to generate the Mono-25, Mono-25′ and Di-pro states using the LEaP module in AMBER 7.0 software package [16].

It should be noted that the X-ray structure of the double mutant, G48V/L90MSQV complex (1FB7) could be considered as an alternative template [4]. However, the X-ray coordinates of the second monomer of the double mutant are not available. Thus, 1HXB is considered to be more appropriate as a template. The mutant protease enzyme was modeled from this structure replacing glycine by valine at residue 48 (G48V) using the Insight II molecular modeling software.

2.2. Molecular dynamics simulations

Three MD simulations were carried out for the mutant HIV-1 PR complexed with saquinavir in the above mentioned states. The Mono-25, Mono-25′ and Di-pro systems were solvated by 9633, 9627 and 9627 TIP3P water molecules [18], respectively. The crystallographic waters were also included in the simulations. The sodium and chloride ions were added to

neutralize the system. The corresponding cubical cell for the three systems was 76 Å × 79 Å × 68 Å. Furthermore, potential parameters for saquinavir are not available in the AMBER package were developed using the following steps. Geometry of the X-ray saquinavir inhibitor was optimized at the Hartree–Fock level with 6-31G** basis functions to adjust the bond-length involving hydrogens. Then, the RESP fitting procedure was employed to calculate partial atomic charges of the inhibitor [19]. Energy minimizations were carried out to relax the model prior to MD runs. A cutoff distance of 12 Å was applied for non-bonded pair interaction. The Particle Mesh Ewald (PME) method was employed for correcting electrostatic interaction. The SHAKE algorithm [20] was employed to constrain all bonds involving hydrogens. The simulated time step was set to 2 fs. The temperature of the model was gradually raised to 298 K during the first 60 ps, then, kept constant until 1 ns.

The molecular mechanics potential energy minimizations and MD simulations were carried out using the AMBER 7.0 simulation package. Calculations were performed using the parm99 force field. All MD runs reported here were done under an isobaric–isothermal ensemble (NPT) using constant pressure of 1 atm and constant temperature of 298 K [21]. All properties reported and discussed in this study were evaluated after equilibrium was reached, 400 ps.

2.3. Quantum chemical calculations

Quantum chemical calculations were performed to investigate the interaction energy between catalytic residues (Asp25 and Asp25′) and saquinavir in the different protonated states of the complexes using the Gaussian 98 program [22]. Initial structures of the complex in the three protonation states were averaged from the whole trajectory, then, the geometry was relaxed using energy minimization from the AMBER 7.0 program. The selected residues, Asp25 and Asp25′, were capped by CH_3NH– and –$COCH_3$ groups at the C- and the N-terminal, respectively. The geometry of the hydrogen atoms in the cap methyl group were optimized using semi-empirical calculations at the PM3 level. Then, single point calculation with the density functional theory B3LYP was applied to investigate the total energy of the system. The basis sets used are the 6-31G(d,p) for unprotonated residue and the extended 6-31+G(d,p) for protonated residue. The total interaction energy of the complex (ΔE_{cpx}) was computed as

$$\Delta E_{cpx} = E_{cpx} - (E_{SQV} + E_{Asp25} + E_{Asp25'}) \quad (1)$$

where E on the right hand side represents total energy of the systems given in the subscript (cpx = complex and SQV = saquinavir). Evaluations were also performed to understand the contribution of pair interactions, $\Delta E_{Asp25-SQV}$, $\Delta E_{Asp25'-SQV}$ and $\Delta E_{Asp25-Asp25'}$, to the total complexation energy, i.e.,

$$\Delta E_{cpx} = \Delta E_{Asp25-SQV} + \Delta E_{Asp25'-SQV} + \Delta E_{Asp25-Asp25'} + \Delta E_{3bd} \quad (2)$$

where the ΔE_{3bd} denotes an error due to three-body correction. In other words, the third particle was excluded from the calculation of the pair interactions which are defined as

$$\Delta E_{Asp25-SQV} = E_{Asp25+SQV} - (E_{Asp25} + E_{SQV}) \quad (3a)$$

$$\Delta E_{Asp25'-SQV} = E_{Asp25'+SQV} - (E_{Asp25'} + E_{SQV}) \quad (3b)$$

$$\Delta E_{Asp25-Asp25'} = E_{Asp25+Asp25'} - (E_{Asp25} + E_{Asp25'}). \quad (3c)$$

In addition to the complexation energy shown in Eq. (1), the interaction energies between saquinavir and the catalytic dyad residues ($\Delta E_{SQV-(Asp25+Asp25')}$) was calculated separately according to the following equation:

$$\Delta E_{SQV-(Asp25+Asp25')} = E_{cpx} - (E_{Asp25+Asp25'} + E_{SQV}) \quad (4)$$

where $E_{Asp25+Asp25'}$ is total energy of the Asp25 and Asp25′ dimer.

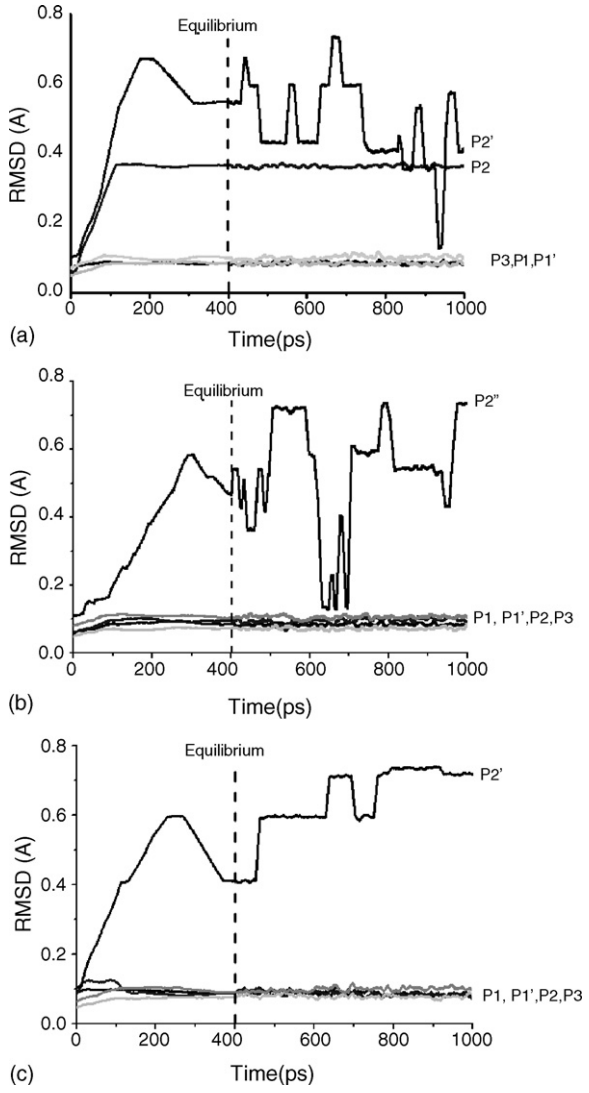

Fig. 2. Root-mean-square displacement (RMSD) of each subsite of saquinavir (defines in Fig. 1d) for the three simulated systems, (a) Mono-25, (b) Mono-25′ and (c) Di-pro.

3. Results and discussion

3.1. Flexibility of the saquinavir inhibitor

The structure of saquinavir is known to consist of five subsites (P1, P2, P3, P1′ and P2′ in Fig. 1d). The root-mean-square displacement (RMSD) of the backbone atoms of each subsite with respect to the starting coordination, the X-ray structure, is plotted in Fig. 2 and the distribution of torsional angle (labeled by *tor* in Fig. 1d) was plotted in Fig. 3. Evaluations were carried out for each subsite of the three protonation states. Note that due to the rigid nature of the planar P1′ subsite, therefore, its torsional plot was not taken into consideration. The RMSD plots through the simulation time indicate clearly that conformations of all subsites in the three protonated states are almost unchanged, except for the P2 subsite of Mono-25 and P2′ subsite in all states.

As a result of these observations, attention was focused on P2 and P2′ subsites. The RMSD plot for P2 subsite for the Mono-25 state (Fig. 2a) is significantly higher than the other two states and the plot for P2′ for the three states are highly flexible when compared with the other subsites. The first event indicates a change of P2 subsite of Mono-25 from one (RMSD ∼0.05 Å) to another (RMSD ∼0.36 Å) conformation (more details are discussed later). Furthermore, the high flexibility of P2′ subsite for all protonation states (Fig. 2a–c) seems to indicate the detection of three preferential conformations for this subsite of saquinavir, e.g., at RMSDs ca. 0.4, 0.6 and 0.7 Å for Di-pro system, etc. This assumption was confirmed by the plot shown in Fig. 4.

Detailed information on the conformational flexibility of each subsite of saquinavir can be seen in terms of distributions of the torsional angles (Fig. 3) after equilibrium, defined in Fig. 1d. All plots show pronounced and sharp peaks indicating slight flexibility of each subsite in a narrow range. For P2′ (Fig. 3c) and P3 (Fig. 3d) subsites, their conformations are not sensitive to the change of protonation states, leading to the most probable torsional angles of 0° and 180°, respectively. Fig. 3b, the torsional angle of P2 subsite of the Mono-25 of ∼90° (solid line, Fig. 3b) differs substantially from that of ∼−75° for the other two states. The difference between the positions of the two peaks, ∼166°, suggests that the orientation of the P2 subsite of saquinavir in the Mono-25 state complex is almost opposite to that of the other states. This statement is supported by the snapshot shown in an inset of Fig. 3b. Note that single preferential conformation after equilibrium of P2 subsite for the Mono-25 state took place at the torsion angle of ∼90° (solid line, Fig. 3b) is consistence with the RMSD = 0.36 Å shown in Fig. 2a. Furthermore, the sharp peak at the torsional angles of ∼−75° for the Mono-25′ and Di-pro (Fig. 3b) states corresponds to the conformation represented by the RMSDs of ∼0.08 Å (Fig. 2b and c).

It is interesting to note that, the observed conformation of P2 subsite of saquinavir in the Mono-25 state is similar to the X-ray structure found in the double mutant, G48V/L90M, HIV-1 PR complex [4]. It was also proposed by the X-ray data that

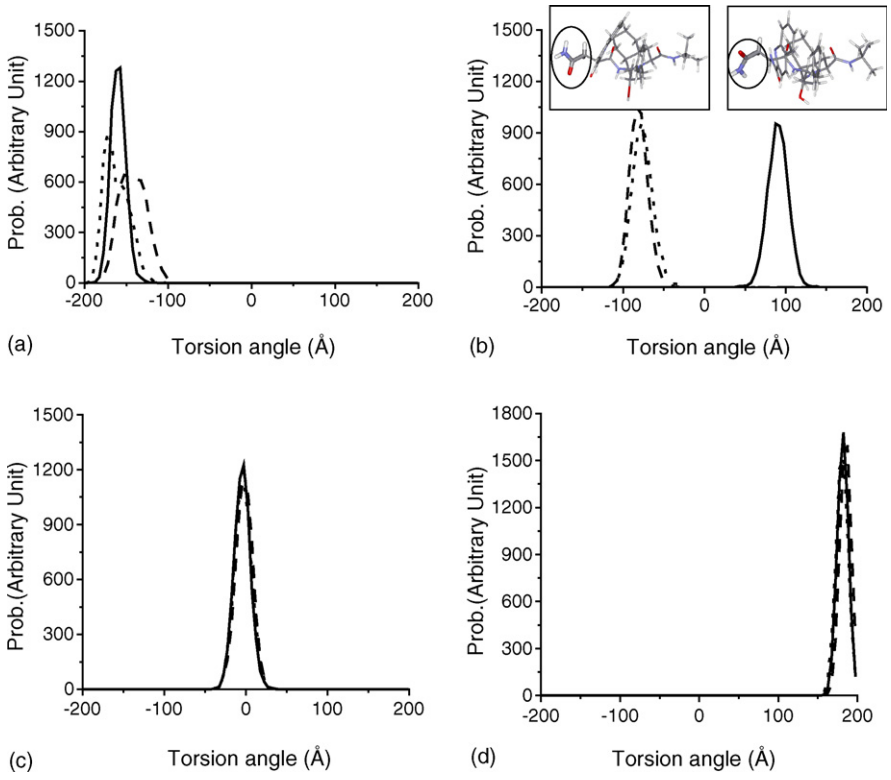

Fig. 3. Changes of torsional angles of four subsites of saquinavir inhibitor: (a) P1 subsite; (b) P2 subsite; (c) P2′ subsite; (d) P3 subsite, (defined in Fig. 1d) for the three simulated systems where solid, dashed and dotted lines in the torsional angle plots represent the Mono-25, Mono-25′ and Di-pro systems, respectively. The two conformations corresponding to torsional angles of 90.3° and −75.5° of P2 are also given in an inset.

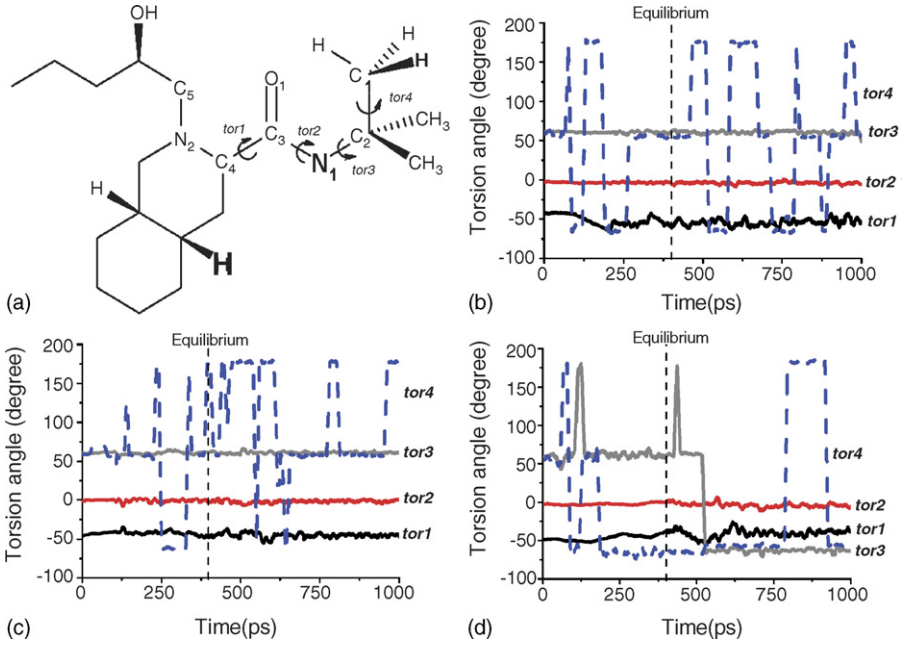

Fig. 4. Definition of torsional angles *tor1–tor4* (a) of the P2′ subsite of saquinavir inhibitor and their changes as a function of simulation time; (b) Mono-25; (c) Mono-25′; (d) Di-pro.

rotation of the P2 subsite of saquinavir in the G48V/L90M mutation depends only on the position of Gly48 which lies much closer to the inhibitor than the Leu90. However, X-ray structure for the present system (single G48V mutation of HIV-1 PR complexed with saquinavir) are not available.

In addition, the three peaks of P1 subsite for the three states are slightly different (Fig. 3a). A sharper and higher peak at the torsional angle of −157° (Mono-25, solid line) than the other at −172° (Di-pro, dot line) and −142° (Mono-25′, dash line) indicate a higher rigidity of P1 subsite in the Mono-25 than the other two states.

To seek more information on the high flexibility of P2′ subsite, the four possible torsional angles, *tor1* (N_2–C_4–C_3–O_1), *tor2* (O_1–C_3–N_1–C_2), *tor3* (C_3–N_1–C_2–C_1) and *tor4* (N_1–C_2–C_1–H) were defined (Fig. 4a) and evaluated. The results were plotted in Fig. 4b–d. The *tor1* and *tor2* for all protonated states are highly stable showing preferential orientations at approximately −50° and 0°, respectively. These results suggested that the –C_3=O_1 functional group of P2′ subsite (see Fig. 4a) was tilted by 50° from the C_3–C_4–N_2 plan while C_2 was detected to locate almost in the O_1–C_3–N_1 plane (*tor2* = 0°). Fluctuations were observed for *tor3* of Di-pro and *tor4* for all states. Particular, *tor4* shows three preferential conformations at −60°, 60° and 180°. This fact can be understood by a free rotation of the –H_3 and –(CH_3) functional groups. An appearance of *tor4* at the three torsional angles for all states indicates a staggered conformation among the three hydrogen atoms of the –CH_3. The same conclusion can also be made for *tor3* of the diprotonated state, Di-pro, in which the three –CH_3 groups are observed to rotate freely with the three preferential states in the staggered conformation.

3.2. Flexibility of enzyme

The RMSD of all atoms with respect to the starting geometry as a function of simulation time was evaluated separately for each chain of the HIV-1 PR. The results were shown in Fig. 5. The plots describe the structure relaxations when the molecule was dissolved in the solution. The RMSD values of all plots increase rapidly for the first 100 ps indicating a change in

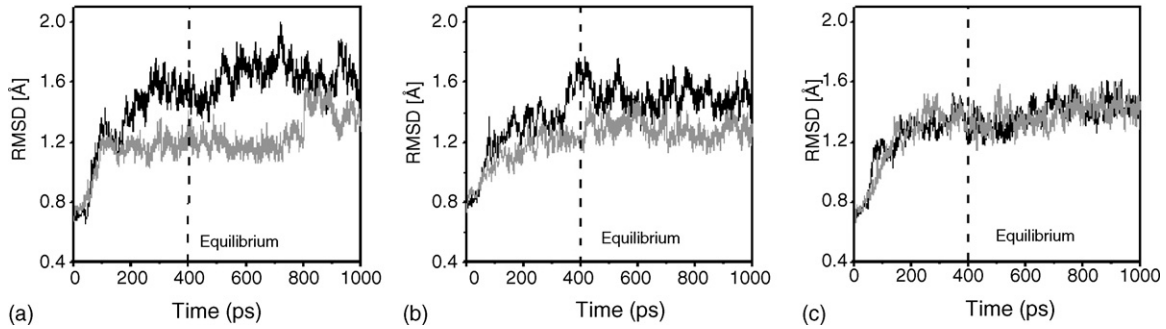

Fig. 5. RMSD as a function of simulation time of the two chains, A (black line) and B (gray line), of the G48V HIV-1 PR mutant-type complexed with saquinavir in the Mono-25 (a), Mono-25′ (b) and Di-pro (c) states.

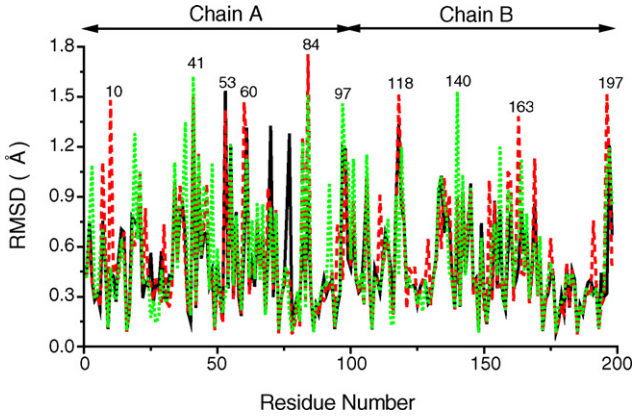

Fig. 6. Root-mean-square deviation for all residues average during 400–1000 ps of the Mono-25 (black), Mono-25′ (red) and Di-pro (green) states where the highly flexible residues were labeled.

enzyme geometry relative to the starting X-ray structure. Although the value of almost all plots remain constant after 200 ps, however, the RMSDs for chain A of Mono-25 (Fig. 5a) and both chains of Mono-25′ still increase slowly (Fig. 5b). This data suggest that monoprotonated states, Mono-25 and Mono-25′, require longer time than the Di-pro state to approach equilibrium. To enhance the reliability of the data, all systems were considered to be in equilibrium after 400 ps. Cooperative effects due to different protonation states and a systematic geometry of the saquinavir inhibitor lead to higher RMSD on chain A (Fig. 5a and b) when compared with chain B of the two monoprotonated states. This difference was not detected for the diprotonated state (Fig. 5c) where both catalytic residues, Asp25 and Asp25′ were protonated.

To ascertain for more details on the flexibility of each residue in the enzyme structure, the RMSD of all atoms for each residue were calculated and displayed in Fig. 6. From the plot, the following conclusions can be made (i) for monoprotonated states, the flexibility of chain A is higher than that of chain B Fig. 6. From the plot, the RMSD of almost all residues of the Mono-25 is slightly lower than those of the Mono-25′ and the Di-pro. The exception was found only for the residues 70 and 71 in which their RMSDs are significantly higher than the other two states. In addition, the highly flexible residues were labeled in Fig. 6. Note that these residues, except residue 84 in which mutation usually takes place, were found to be located on the solvent accessible surface of the enzyme.

3.3. Enzyme–saquinavir interaction

It is well known that inhibitor or substrate was held in the active site of enzyme via the intermolecular forces, such as electrostatic, hydrophobic, dispersion forces, etc. For the investigated system where the hydrophilic OH group of saquinavir binds directly to the catalytic residues, the catalytic region contains residues 25–30: Asp25-Thr26-Gly27-Ala28-Asp29-Asp30 and some water molecules. It appears that the electrostatic forces in the catalytic pocket play a key role of the complex. Therefore, attention was focused on the hydrogen bonding between inhibitor and enzyme. In addition, interaction between saquinavir and the catalytic dyad was also investigated.

Hydrogen bonding between HIV-1 PR and saquinavir was determined based on the Carnel module in the AMBER 7.0 using the following criteria: (i) the distance between proton donor (D) and acceptor (A) atoms was less than or equal to 3.5 Å and (ii) the D−H···A angle was greater than or equal to 120°. Analysis was carried out cover the entire trajectory after equilibration. The detected hydrogen bonds with the H···A distances were shown in Fig. 7a–c. It is interesting to note that hydrogen bonds between saquinavir and HIV-1 PR were formed only in the two regions that are flap and active site region. The number of hydrogen bonds were found 4, 5 and 6 for the Mono-25, Mono25′ and Di-pro states, respectively. In the flap region, hydrogen bonds were formed only with the Val48 of the HIV-1 PR. In the Mono-25 state (Fig. 7a), the deformation of *d5* bond (5.75 Å) was observed. This observation is due to the rotation of the NH_2 functional group of P2 subsite of saquinavir (inset of Fig. 3b). In addition, the

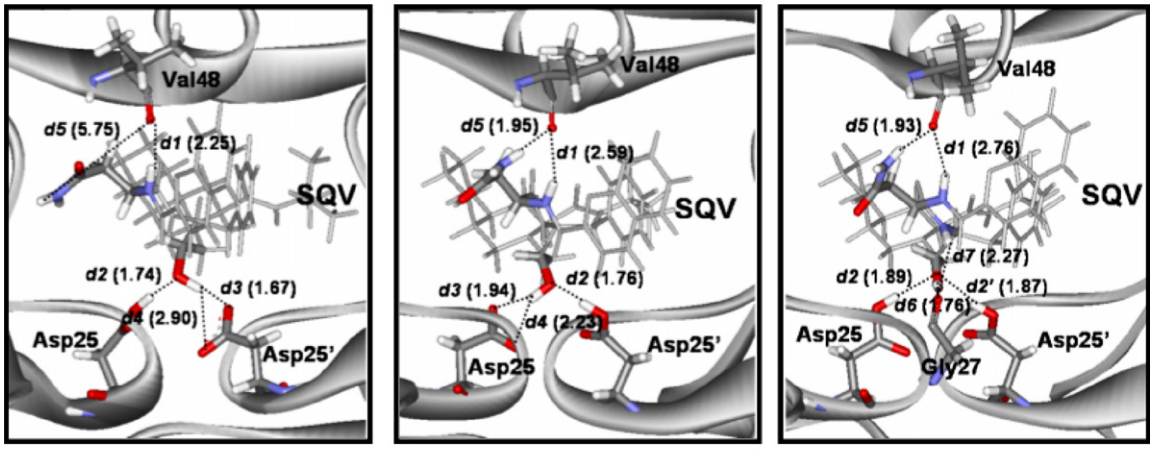

(a) (b) (c)

Fig. 7. Detected hydrogen bonds (dash line) in the HIV-1 PR enzyme–saquinavir complex in (a) Mono-25, (b) Mono-25′ and (c) Di-pro states, where the average hydrogen bond distances (H···A distance) in Å are numbered.

remaining hydrogen bond (*d1*) at the average distance of 2.25 Å is slightly stronger than those of 2.59 and 2.76 Å for the Mono-25′ and Di-pro states, respectively. For the active site region of the two monoprotonated states, the OH functional group of saquinavir was found to form three hydrogen bonds (*d2–d4*) with the two catalytic residues in which, one hydrogen bond with the protonated and the other two with the unprotonated carbonyl group. An exception was found for the Di-pro state where, the unprotonated group is not available, therefore, the other bond was formed with Gly27 (*d6* and *d7* in Fig. 7c).

Furthermore, indirect binding between saquinavir and the three residues, Gly27, Asp29 and Asp30, of the HIV-1 PR via the hydrogen bonds through water molecules was detected and displayed in Fig. 8. In the Mono-25 state (Fig. 8a), the conformation of P2 subsite was found to rotate and indirectly bind to the three residues of enzyme. The oxygen atom and hydrogen atom of P2 subsite form hydrogen bonds with Asp29 and Gly27 via two water molecules and with Asp30 via one water molecule (Fig. 8a), respectively. Even though those hydrogen bonds were not detected for Mono-25′. However, the nitrogen atom of the NH_2 group of P2 subsite for Mono-25′ was found to form a hydrogen bond with Asp30 via one water molecule (Fig. 8b), instead.

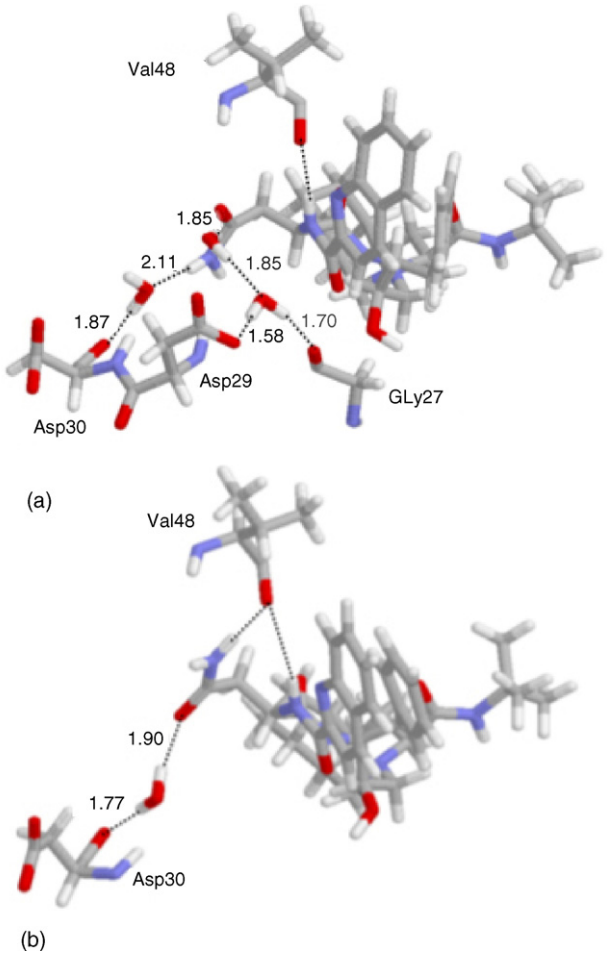

Fig. 8. Indirect binding between HIV-1 PR and saquinavir via hydrogen bonds (dash line) through water molecules in the (a) Mono25 and (b) Mono-25′ states where the average distance (in Å) are numbered.

To evaluate the interaction between saquinavir and the catalytic residues, quantitatively, DFT calculations were performed. The total complexation energy (ΔE_{cpx}), interaction between saquinavir and catalytic dyad ($\Delta E_{SQV-(Asp25+Asp25')}$) and pair interactions as well as error due to three-body effects (ΔE_{3bd}) are summarized in Table 1a (see method of calculation for more details).

The average RMSDs of the ASP25 and ASP25′ residues for the three investigated systems with the deviations of less than 0.16 Å were summarized in Table 1b. This indicates reliability of the DFT energy calculations in which the MD snapshots can be represented by the average structure.

In terms of complexation energies, the obtained order of the ΔE_{cpx} is Mono-25 > Mono-25′ > Di-pro, i.e., interaction energy of −37.3 kcal/mol for the Mono-25 state is significantly lower than those of −30.7 and −10.7 kcal/mol for the Mono-25′ and Di-pro states, respectively. This evidence is in good agreement with that previously reported for saquinavir complexed with wild-type HIV-1 PR in which only Asp25 monoprotonated state is in the reasonable binding affinity [17,23,24]. In addition, quantum mechanics and molecular mechanics calculations [12] for the HIV-1 PR-74704 inhibitor complex leads also to the conclusion that the protonated state of the active site of the complex is monoprotonated state on Asp25.

In Table 1a, the total complexation energy (ΔE_{cpx}) can be separated into three terms of pair interaction and additional three-body correction terms. As expected, the main contribution to complexation energy is due to the electrostatic interactions between saquinavir and non-protonated state aspartic acids which amount to −19.2 and −18.0 kcal/mol for the Mono-25 and Mono-25′, respectively. In addition, interactions with the two protonated residues are −8.0 kcal/mol for both Mono-25 and Mono-25′. Summation of the two terms of the pair interaction, $\Delta E_{SQV-Asp25}$ and $\Delta E_{SQV-Asp25'}$, yields the total interaction of −28.4 kcal/mol for Mono-25 and −28.0 kcal/mol for Mono-25′. These two values are almost consistent with the total interaction between saquinavir and the two aspartic residues calculated from $\Delta E_{SQV-(Asp25+Asp25')}$. The difference is due to many-body correction term, Asp25′ and Asp25 were excluded in the calculation of the $\Delta E_{SQV-Asp25}$ and $\Delta E_{SQV\text{-}Asp25'}$, respectively. Taking into account the data summarizing above, no significant difference was found among the interaction between saquinavir and the catalytic residues of the HIV-1 PR of the two mono-protonated states.

Table 1a
Interaction between saquinavir (SQV) and the catalytic residues, Asp25 and Asp25′, of HIV-1 PR for the three protonated states yielded from ab initio calculations (see text for more details)

Interaction energy (kcal/mol)	Mono-25	Mono-25′	Di-pro
ΔE_{cpx}	−37.3	−30.7	−10.7
$\Delta E_{SQV-(Asp25+Asp25')}$	−28.4	−28.0	−11.5
$\Delta E_{Asp25-SQV}$	−8.0	−18.0	−6.2
$\Delta E_{Asp25'-SQV}$	−19.2	−8.0	−7.9
$\Delta E_{Asp25-Asp25'}$	−8.8	−2.6	+0.8
ΔE_{3bd}	−1.2	−2.1	+2.6

Table 1b
Average RMSDs as well as their deviations for the ASP25 and Asp25′ of the Mono-25, Mono-25′ and Di-Pro systems evaluated after equilibration, 400–1000 ps

Res. no.	Mono-25		Mono-25′		Di-pro	
	RMSD	Deviation	RMSD	Deviation	RMSD	Deviation
Asp25	0.56	0.10	0.38	0.08	0.18	0.05
Asp25′	0.37	0.06	0.47	0.12	0.35	0.16

Interest is focused on the Asp25–Asp25′ interaction which was observed to be the key contribution to the ΔE_{cpx}, leading to a much lower ΔE_{cpx} in the Mono-25 than that of the Mono-25′. A significantly lower Asp25–Asp25′ interaction energy of −8.8 kcal/mol for the Mono-25 than that of −2.6 kcal/mol for the Mono-25′ suggests us to make a clear conclusion that protonation at the Asp25 leads to a better arrangement in the catalytic dyad. Interestingly, such rearrangement does not make any difference on the $\Delta E_{SQV-Asp25}$ or $\Delta E_{SQV-Asp25'}$ interactions (Table 1a) in comparison between the two monoprotonated residues. This finding also agrees well with the hydrogen bond formation between saquinavir and catalytic residues of the Mono-25 and Mono-25′ where three hydrogen bonds were observed and the hydrogen bond distance for the two systems are almost equivalent, *d2*, *d3* and *d4* in Fig. 7.

Furthermore, rearrangement of the catalytic dyad was supposed to be the source of conformation change of the P2 subsite of saquinavir in the Mono-25 state (Fig. 3) and of the vanishing of one hydrogen bond between Val48 and saquinavir in the flap region (Fig. 7a).

The above data suggest us to conclude that interaction in the catalytic site should be used as criteria to enhance capability in drug designing and drug screening instead of using the total inhibitor/enzyme interaction. In addition, interaction between the inhibitor and the catalytic region of the enzyme is supposed to relate directly to the activity of the inhibitor in the catalytic process.

4. Conclusions

We have reported a result of 1 ns molecular dynamic (MD) simulation of three protonation states (Mono-25, Mono-25′ and Di-pro) for G48V mutant HIV-1 PR complexed with the saquinavir inhibitor. Detailed analyses of structure and dynamics characters among the three protonation states of G48V mutant were given in terms of the flexibility, hydrogen bonding and conformational changes as well as binding energy between inhibitor and enzyme. The results indicate that the three complexes display a distinct dynamical behavior. A major structure change via complexation was found at P2 subsite of saquinavir which affected the hydrogen bonding for enzyme–inhibitor interaction and water molecule. The interaction data yielded from quantum chemical calculations supports the previous conclusion which state that the protonated state of the active site of the mutant-type HIV-1 PR complexed with saquinavir is a monoprotonated state on Asp25 (Mono-25). The energy data indicate also that protonation at the Asp25 lead to a better arrangement in the catalytic dyad. In addition, conformation of the P2 subsite in the Mono-25 is consistent with that obtained from the X-ray structure of G48V/L90M mutant HIV-1 PR complexed with saquinavir.

Acknowledgments

We are very grateful to the Computational Chemistry Unit Cell and the Austrian-Thai Center for Computer Assisted Chemical Education and research (ATC), Department of Chemistry, Faculty of Science, Chulalongkorn University, Thailand for the use of computer resources. This work was supported by Thailand Research Fund Senior Scholar, Grant No. RTA468008.

Appendix A. Supplementary data

Supplementary data associated with this article can be found, in the online version, at doi:10.1016/j.jmgm.2006.01.004.

References

[1] CDC, First report of AIDS, MMWR 30 (1981) 250–252.
[2] B. Mahalingam, J.M. Louis, J. Hung, R.W. Harrison, I.T. Weber, Structural implications of drug-resistant mutants of HIV-1 protease: high-resolution crystal structures of the mutant protease/substrate analogue complexes, Proteins 43 (2001) 455–464.
[3] T. Skalova, J. Hasek, J. Dohnalek, H. Petrokova, E. Buchtelova, J. Duskova, M. Soucek, P. Majer, T. Uhlikova, J. Konvalinka, An ethylenamine inhibitor binds tightly to both wild type and mutant HIV-1 proteases. Structure and energy study, J. Med. Chem. 46 (2003) 1636–1644.
[4] L. Hong, X.C. Zhang, J.A. Hartsuck, J. Tang, Crystal structure of an in vivo HIV-1 protease mutant in complex with saquinavir: insights into the mechanisms of drug resistance, Protein Sci. 9 (2000) 1898–1904.
[5] R.W. Shafer, P. Hsu, A.K. Patick, C. Craig, V. Brendel, Identification of biased amino acid substitution patterns in human immunodeficiency virus type 1 isolates from patients treated with protease inhibitors, J. Virol. 73 (1999) 6197–6202.
[6] C.F. Shuman, P.-O. Markgren, M. Hämäläinen, U.H. Danielson, Elucidation of HIV-1 protease resistance by characterization of interaction kinetics between inhibitors and enzyme variants, Antiviral Res. 58 (2003) 235–242.
[7] R. Kantor, W.J. Fessel, A.R. Zolopa, D. Israelski, N. Shulman, J.G. Montoya, M. Harbour, J.M. Schapiro, W.R. Shafer, Evolution of primary protease inhibitor resistance mutations during protease inhibitor salvage therapy, Antimicrob. Agents Chemother. 46 (2002) 1086–1092.
[8] A. Wlodawer, J.W. Erickson, Structure-based inhibitors of HIV-1 protease, Annu. Rev. Biochem. 62 (1933) 543–585.
[9] J. Ermolieff, X. Lin, J. Tang, Kinetic properties of saquinavir-resistant mutants of human immunodeficiency virus type 1 protease and their implications in drug resistance in vivo, Biochemistry 36 (1997) 12364–12370.
[10] S. Piana, D. Sebastiani, P. Carloni, M. Parrinello, Ab initio molecular dynamics-based assignment of the protonation state of pepstatin A/HIV-1 protease cleavage site, J. Am. Chem. Soc. 123 (2001) 8730–8737.
[11] R. Smith, I.M. Brereton, R.Y. Chai, S.B. Kent, Ionization states of the catalytic residues in HIV-1 protease, Nat. Struct. Biol. 3 (1996) 946–950.
[12] K.-Y. Nam, B.H. Chang, C.K. Han, S.G. Ahn, K.T. No, Investigation of the protonated state of HIV-1 protease active site, Bull. Korean Chem. Soc. 24 (2003) 817–823.
[13] Z. Zhu, D.I. Schuster, M.E. Tuckerman, Molecular dynamics study of the connection between flap closing and binding of fullerene-based inhibitors of the HIV-1 protease, Biochemistry 42 (2003) 1326–1333.

[14] A. Krohn, S. Redshaw, J.C. Ritchie, B.J. Graves, M.H. Hatada, Novel binding mode of highly potent HIV-proteinase inhibitors incorporating the (*R*)-hydroxyethylamine isostere, J. Med. Chem. 34 (1991) 3340–3342.

[15] W.A.K.P.A. Wang, Computational study of protein specificity: the molecular basis of HIV-1 protease drug resistance, PNAS 98 (2001) 14937–14942.

[16] D.A. Case, J.C.D. Pearlman, T. Cheatham III, J. Wang, W. Ross, C. Simmerling, T.D.T. Merz, R. Stanton, A. Cheng, J. Vincent, M. Crowley, V.T.H. Gohlke, R. Radmer, Y. Duan, J. Pitera, I. Massova, G. Seibel, U.C.S.P. Weiner, P.A. Kollman, AMBER 7, University of California, San Francisco, CA, 2002.

[17] K. Wittayanarakul, O. Aruksakunwong, S. Saen-oon, W. Chantratita, V. Parasuk, P. Sompornpisut, S. Hannongbua, Insights into saquinavir resistance in the G48V HIV-1 protease: quantum calculations and molecular dynamic simulations, Biophys. J. 88 (2005) 867–879.

[18] W.L. Jorgensen, J. Chandrasekhar, J.D. Madura, Comparison of simple potential functions for simulating liquid water, J. Chem. Phys. 79 (1983) 926–935.

[19] C.I. Bayly, P. Cieplak, W.D. Cornell, P.A. Kollman, A well-behaved electrostatic potential based method using charge restraints for determining atom-centered charges: the RESP model, J. Phys. Chem. 97 (1993) 10269.

[20] J.P. Ryckaert, G. Ciccotti, H.J.C. Berendsen, Numerical integration of the cartesian equations of motion of a system with constraints: molecular dynamics of *n*-alkanes, J. Comput. Phys. 23 (1977) 327–341.

[21] H.J.C. Berendsen, J.P.M. Postma, W.F.V. Gunsteren, A. DiNola, J.R. Haak, Molecular dynamics with coupling to an external bath, J. Chem. Phys. 81 (1984) 3684–3690.

[22] M.J. Frisch, G.W. Trucks, H.B. Schlegel, G.E. Scuseria, M.A. Robb, J.R. Cheeseman, V.G.J.A.M. Zakrzewski Jr., R.E. Stratmann, J.C. Burant, S. Dapprich, J.M. Millam, A.D. Daniels, K.N. Kudin, M.C. Strain, O. Farkas, J. Tomasi, V. Barone, M. Cossi, R. Cammi, B. Mennucci, C. Pomelli, C. Adamo, S. Clifford, J. Ochterski, G.A. Petersson, P.Y. Ayala, Q. Cui, K. Morokuma, D.K. Malick, A.D. Rabuck, K. Raghavachari, J.B. Foresman, J. Cioslowski, J.V. Ortiz, A.G. Baboul, B.B. Stefanov, G. Liu, A. Liashenko, P. Piskorz, I. Komaromi, R. Gomperts, R.L. Martin, D.J. Fox, T. Keith, M.A. Al-Laham, C.Y. Peng, A. Nanayakkara, C. Gonzalez, M. Challacombe, P.M.W. Gill, B. Johnson, W. Chen, M.W. Wong, J.L. Andres, C. Gonzalez, M. Head-Gordon, E.S. Replogle, J.A. Pople, Gaussian 98 Program (Revision A.7). Journal, 1998.

[23] Y. Won, Binding free energy simulations of the HIV-1 protease and hydroxyethylene isostere inhibitors, Bull. Korean Chem. Soc. 21 (2000) 1207–1212.

[24] K. Wittayanarakul, O. Aruksakunwong, P. Sompornpisut, V. Sanghiran-Lee, V. Parasuk, S. Pinitglang, S. Hannongbua, Structure, dynamics and solvation of HIV-1 protease/saquinavir complex in aqueous solution and their contributions to drug resistance: molecular dynamic simulations, J. Chem. Inf. Model. 45 (2005) 300–308.